Biophysical Journal, Volume *114*

Supplemental Information

FSCS Reveals the Complexity of Lipid Domain Dynamics in the Plasma Membrane of Live Cells

Philip R. Nicovich, Joanna M. Kwiatek, Yuanqing Ma, Aleš Benda, and Katharina Gaus

Supplemental Information for: Lifetime of Cellular Membrane Domains Measured by Fluorescence Spectral Correlation Spectroscopy

Philip R Nicovich[*,1,2,3], Joanna M. Kwiatek[*,1,2], Yuanqing Ma[1,2], Aleš Benda[2,3] and Katharina Gaus[1,2]

[1] *EMBL Australia Node in Single Molecule Science, School of Medical Sciences, University of New South Wales, Sydney, Australia.*
[2] *ARC Centre of Excellence in Advanced Molecular Imaging, University of New South Wales, Sydney, Australia*
[3] *Allen Institute for Brain Science, Seattle, Washington, USA*
[4] *Imaging methods core facility at BIOCEV, Faculty of Sciences, Charles University, Průmyslová 595, 252 42 Vestec, Czech Republic*
[*] *These authors shared equally in this work*

FSCS Theory

As presented in (*1*), the principle of FSCS relies on the fact that the spectrum of a mixture of N multiple emissive species at any time t can be described as a linearly-weighted combination of the spectra of the constituent species. This holds true across a given number of j spectral channels, such that

$$I_j(t) = \sum_{i=1}^{N} w_{i,j}(t) p_{i,j}(t) \tag{1}$$

where $I_j(t)$, $w_{i,j}(t)$, and $p_{i,j}(t)$ are the total intensity, weighting coefficient of component i, and pure spectrum of component i, all at time t and in spectral channel j. Given that the number of spectral channels exceeds the number of emissive species and the photon distribution remains Poissonian, single-value decomposition can be applied and Eq 1 can be re-written in terms of the total intensity, weighting coefficient, and a filter coefficient $f_{j,k}(t)$ for spectral channel j and component k.

$$w_k(t) = \sum_{j=1}^{M} f_{j,k}(t) I_j(t) \tag{2}$$

This weighting coefficient $w_k(t)$ here is the more familiar single scalar value result used in spectral unmixing for discerning contributions of separate emitters in spectral confocal imaging or other spectral decomposition techniques.

A matrix of filter coefficients $F(i,j) = f_{j,k}$ can be calculated from straightforward matrix operations given area-normalized spectral for the spectra of each emissive component and the spectrum to be decomposed.

$$F = ([P]^T diag\langle I(t)\rangle_t^{-1})[P])^{-1} [P]^T diag\langle I(t)\rangle_t^{-1} \tag{3}$$

where $P(i,j) = p_{i,j}$, or the area-normalized spectral intensity of pure component i in spectral channel j.

Photons arrivals during the FSCS acquisition are recorded with both the timestamp and the spectral channel in which the photon was detected. A weighting coefficient vector $w_k(t)$ for each constituent component is generated by treating matrix F as a look-up table returning the associated filter coefficient $f_{j,k}$ for channel j and component k. The correlation as a function of lag time τ between the signals from components k and l is then defined as

$$G_{k,l}(\tau) = \frac{\langle w_k(t)\, w_l(t+\tau)\rangle_t}{\langle w_k(t)\rangle_t \langle w_l(t)\rangle_t} \tag{4}$$

where $k = l$ in the case of autocorrelation and $k \neq l$ for cross-correlation. Efficiently calculating correlations can be accomplished through the method described by Wahl (*2*), but where the weight of each photon is given by $w_k(t)$ rather than the usual value of 1 (*3*).

Here each measurement of 180 seconds was split equally into ten time intervals and autocorrelations calculated for each with equal weighting for all spectral channels ($w = 1$ for each photon). The K time segments (here $K = 6$) which correlations most closely matched the mean correlation (assessed as sum of squares difference) were carried forward. The auto- and cross-correlations for those K time segments were then evaluated given the spectral weighting values for the channel in which each photon was detected.

Given the complex diffusion mechanisms anticipated for the samples under study, it is necessary to define a method for timescale analysis that is not dependent on a particular diffusional model. As used in previous work, the $t_{1/2}$ value, or the time for the correlation to decay to half its value at 0 time is appropriate (*1*, *4*). Given the noise in the correlation at short timescales, we substitute the value of the correlation at a range of short lag (τ) values for the value at $\tau = 0$. For data presented in Figure S1 this is the mean value of the correlation at $1x10^{-4} < \tau \leq 5x10^{-4}$ seconds and in Figure 1 $5x10^{-4} < \tau < 5x10^{-3}$ seconds. We point out that for the case of simple two-dimensional diffusion of the form $G(\tau) = (1 + \frac{t}{\tau_D})^{-1}$, one can trivially derive that $t_{1/2} = \tau_D$. Taking into account triplet transitions yields the expression

$$t_{1/2} = \tau_T\, W(z) - 2T\,\tau_D + \tau_D \tag{5a}$$

$$z = 2T\frac{\tau_D}{\tau_T} exp\left[\frac{(2T-1)\tau_D}{\tau_T}\right] \tag{5b}$$

where T is the triplet fraction, τ_T the triplet timescale, and W the Lambert W function. Extending this to three-dimensional diffusion with or without including triplet states becomes quite complex and beyond the scope required here. This expression demonstrates that the value for $t_{1/2}$ is a weighted average of the timescales present in the experiment.

With this estimate for the diffusion timescale τ_D we can use the Stokes-Einstein relationship (6) to yield parameters of the experimental system. Here

$$\frac{\omega_{xy}^{o2}}{4\tau_D} = D = \frac{k_b T}{6\pi\,\eta\,R_h} \tag{6}$$

where k_b is the Boltzmann constant, T temperature, η the environment viscosity, and R_h the radius of hydration of the diffusing species. We estimate the lateral beam waist as $\omega_{xy}^{o2} = \lambda/(1.22\,n\,NA)$ where λ is the excitation wavelength (514 nm), n the refractive index of the medium (1.33) and NA the numerical aperture of the system (1.20). Here this relationship is used in validating model membrane viscosity where the diffusional environment is sufficiently uncomplicated such that the approximation $t_{1/2} \approx \tau_D$ is appropriate. In other cases the value of $t_{1/2}$ is used as a comparison between conditions and not fit to a diffusion model.

Probe distribution and brightness within L_o and L_d environments

Previous work established that NR12S in phase-separated GUVs shows similar preference for the Lo and Ld phases (*5*). It was noted that this behavior is uncommon amongst environmentally-sensitive dyes enhancing the choice of NR12S as a selected probe for these experiments. However the exact preference for one phase versus the other is difficult to establish based on fluorescence intensity alone as the quantum yield of the NR12S fluorophore can vary by nearly a factor of 2 based on the polarizability of the surrounding lipid solvent.

To address the effect on the FSCS results of a possible difference in probe affinity and fluorescence efficiency in different lipid environments we performed additional simulations. In these simulations we kept the probe density and diffusional mode constant, but varied the intensity of the individual probes based on the surrounding environment. At the same time we varied the diffusion constant of the probe within the two membrane environments.

Simulations show that a difference in diffusion constant between the two membrane phases is sufficient to produce a difference in both autocorrelation time and amplitude (manuscript Figure 2D). This occurs with equal abundance of the two simulated phases as well as no environmentally-sensitive difference in probe brightness. In this situation the phase showing a greater value for the simulated diffusion constant will have a lower amplitude than the phase with the lesser value for diffusion constant. In other words, the phase with faster diffusion will have a lower amplitude in the corresponding autocorrelation function given equal phase abundance and probe brightness.

At the same time, it is possible for probe brightness to influence the autocorrelation amplitude. Increasing probe brightness in a given phase relative to the other correspondingly increases the autocorrelation amplitude for that phase.

From the experimental data we observe the Ld phase always having a longer diffusion time than the L_o phase. All experimental systems show a ratio of L_d/L_o autocorrelation amplitudes greater than 1. We expect the L_d autocorrelation to have a greater amplitude than the L_o phase autocorrelation, given equal probe brightness. Varying the simulated probe brightness by a factor of two away from equal is sufficient to reach the cross-over point such that the brighter, faster L_o phase shows a greater autocorrelation amplitude than the slower, dimmer L_d phase (simulated diffusion constants of 0.3 and 0.1 $\mu m^2/sec$ and relative brightness of 2:1 for the L_o and L_d phases, respectively). The converse brightness ratio with the same diffusion constants yields simulated amplitudes in the proper sign but with L_o/L_d autocorrelation amplitudes greater than the majority of the observed experimental data.

While it is difficult to extract an experimental diffusion constant given the complex membrane environment, these data together suggest that the relative brightness of the NR12S probe in the experimental membrane environments is within a factor of 2 of equivalent.

Model systems provide reference spectra for L_o and L_d environments

The sub-diffractive and transitive nature of isolated L_o and L_d regions make collecting *in situ* reference spectra for these domains intractable. Such an experiment would significantly bias the measured spectra towards time-domain-averaged and point-spread-function-blurred of the true spectra of the extreme membrane environments present. Instead we must rely on reference spectra collected in model membrane solutions accepted to produce the desired extrema membrane domain structures. Figure S1 shows these reference spectra for the chosen model domains.

The suitability of these reference spectra for the experimental datasets were evaluated through measuring the resulting error from perturbating these spectra and attempting to fit the experimental data. Spectra for NR12S in reference L_o and L_d are reasonably fit by Gaussian curves. This is clear in the fits of experimental data as well as those appearing

in Reference (*5*). Figure S9A shows data and fits as presented in main manuscript while shows same data and fits with intensities normalized to correct for inhomogeneous spectral bin width. Here the L_o curve has mean = 580.7 nm and σ = 38.8 nm; L_d curve has mean = 615.4 nm, σ = 36.2 nm.

Potential reference spectra were generated from these fits by varying mean values (*i.e.* peak center position) with the other parameters kept constant. Trials were then defined by the peak position of the L_o peak and the distance from there to the L_d peak position (580.7 nm and 34.7 nm in fits, respectively). Representative spectra for each test condition were fit (eq 3) with error defined as cumulative root mean squared distance of the summed filter coefficients from 1.

Results for each test condition shown in S9 C-E with minimum values marked. These minima fall at L_o position/L_o-L_d distance of 585 nm / 35 nm for the Live cell condition, 580 nm /35 nm for the LatB treatment, and 585 nm / 30 nm for the 7KC treatment condition. Each of these values are within 1 bin of the original fit data. Indeed, the bifurcated 'valley' within the data propagating away from the minimum value is further support that the experimental spectra are well-described by this semi-empirical system. Having one or the other domain's spectrum centered near the fit spectrum value produces better fits than having both at more extreme values. The topography of this surface is smooth and demonstrates a continuous approach to an optimum value rather than the chosen spectra carrying critical information not captured by the Gaussian peaks.

The absolute summed rms errors for these minima is 0.2278, 0.2373, or 0.3383 for the control, LatB, and 7KC treatment conditions, respectively. The summed rms error for reference spectra measured in model systems applied to all acquired live-cell experimental spectra is 0.1361 ± 0.0527, 0.1277 ± 0.0395, or 0.2898 ± 0.0504 for the control, LatB, and 7KC treatment conditions (mean ± standard deviation, N = 18, 19, and 10, respectively).

Semi-empirical spectra with positions at or near that derived from spectra of NR12S in the chosen model systems is the best fit for representative experimental data. Errors from using the actual model system spectra are smaller than those from the best-fit semi-empirical result. If a better set of basis spectra existed to fit the experimental data, for example those farther separated than the model system chosen due to more extreme changes in environment, we would expect to see that reflected in the error maps. However, the minimum errors are found using spectra from the model membrane systems. As such we can conclude that the NR12S spectra in the chosen model systems are at or near the optimum basis spectra from which to unmix the signals measured across all of the live cell experiments in this work.

References

1. A. Benda, P. Kapusta, M. Hof, K. Gaus, *Opt. Express* **22**, 2973–2988 (Feb. 2014).
2. M. Wahl, I. Gregor, M. Patting, J. Enderlein, *Opt. Express* **11**, 3583–3591 (Dec. 2003).
3. D. Waithe, M. P. Clausen, E. Sezgin, C. Eggeling, *Bioinformatics*, DOI: 10.1093/bioinformatics/btv687, eprint: http://bioinformatics.oxfordjournals.org/content/early/2015/11/19/bioinformatics.btv687.full.pdf+html (2015).
4. Y. Ma, A. Benda, P. R. Nicovich, K. Gaus, *Biomed. Opt. Express* **7**, 1561–1576 (Apr. 2016).
5. O. A. Kucherak *et al.*, *J. Am. Chem. Soc.* **132**, 4907–4916 (Apr. 2010).

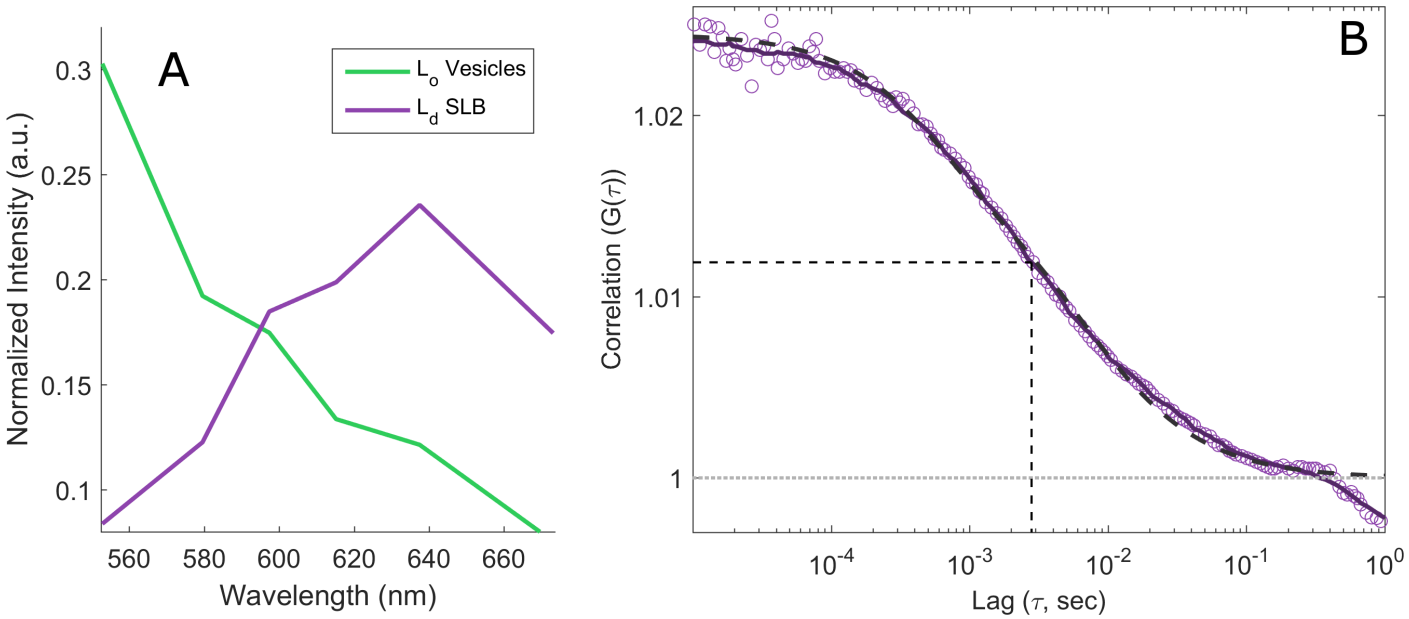

Figure S1: **NR12S in single-phase lipid samples**. A) Spectra of NR12S in single-phase samples. B) Autocorrelation (circles) and smoothed curve (solid line) for NR12S in L_d supported lipid bilayers (D, purple). The $t_{1/2}$ amplitude and time is indicated in each panel as a dashed black line.

Cell Condition	L_o lifetime (mean [95 % CI], ms)	L_d lifetime (mean [% CI], ms)
Control	5.90 [2.93 - 55.52]	14.69 [4.11 - 93.8]
7KC	6.48 [1.97 - 39.70]	24.38 [4.56 - 67.03]
LatB	5.15 [1.80 - 50.27]	13.13 [2.09 - 47.83]

Table S1: **Domain lifetimes by treatment condition.**

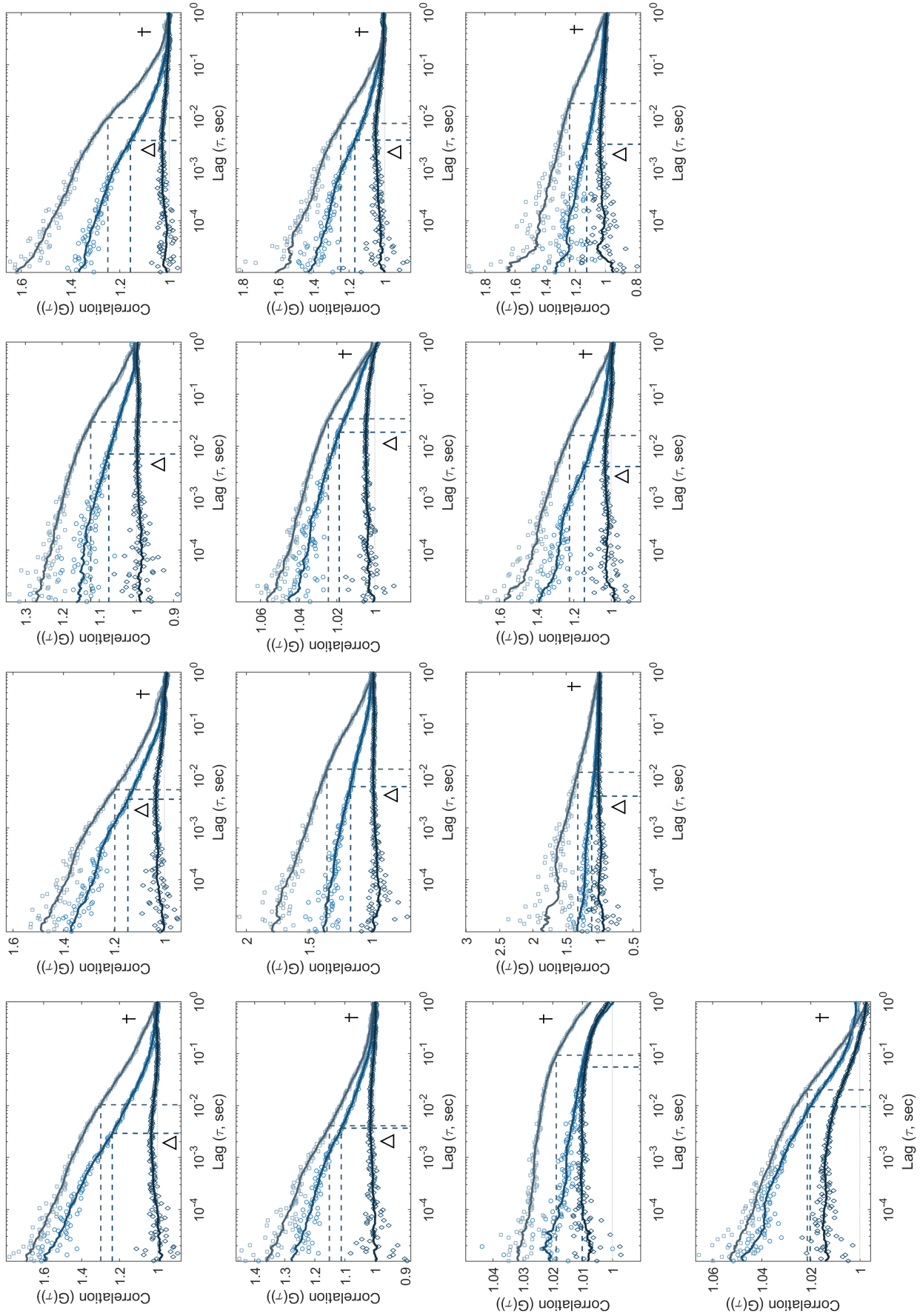

Figure S2: **Correlation results from live COS7 cells stained with NR12S**. Dagger annotations (†) indicate those cross-correlations with positive or negligible cross-correlation signal at $\tau > 10^{-4}$. Triangle annotations (△) indicate those cross-correlations with peaks on the timescale of the autocorrelation decay ($10^{-4} < \tau < 10^{-1}$).

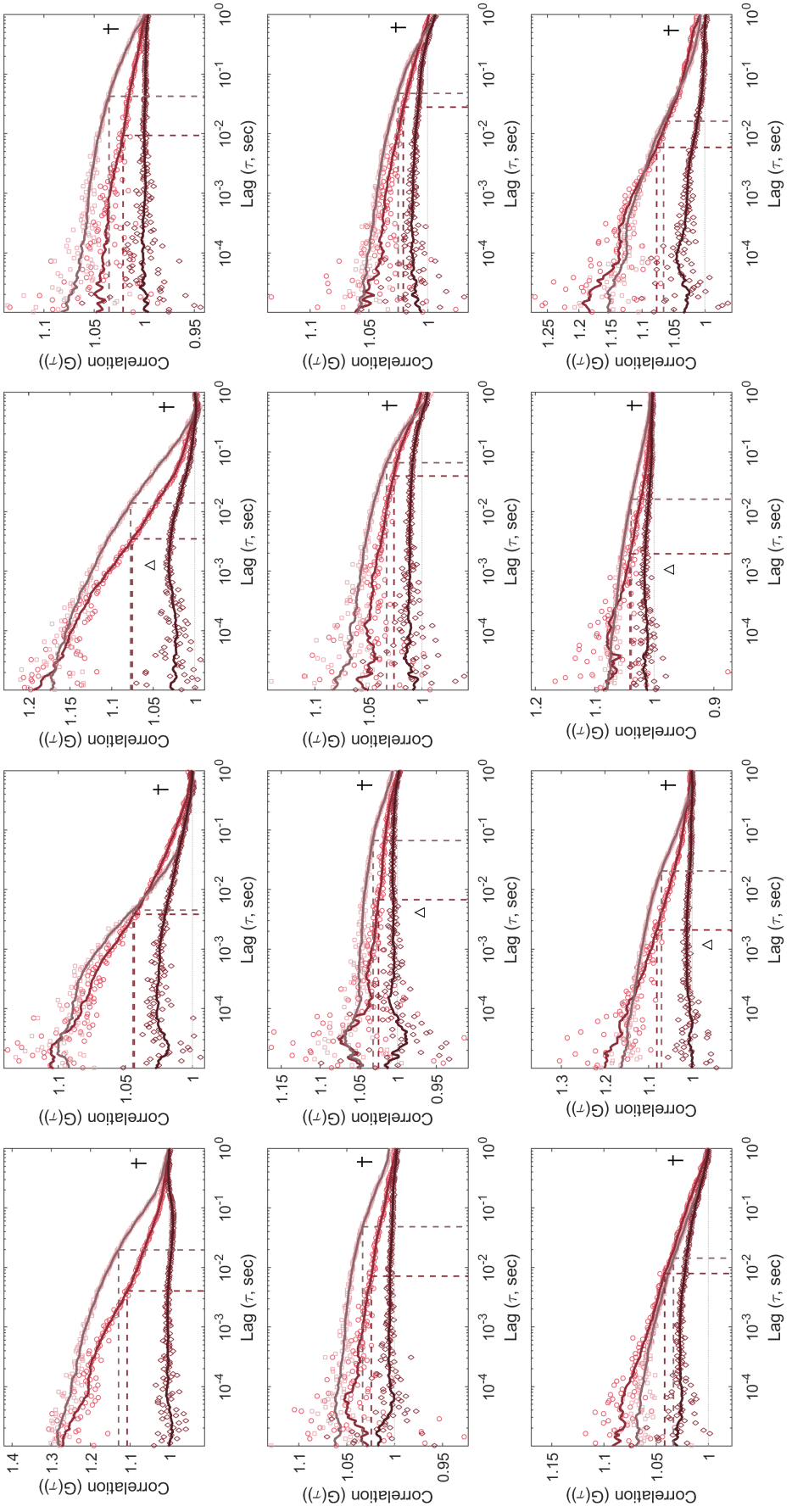

Figure S3: **Correlation results from 7KC-treated cells stained with NR12S**. Dagger annotations (†) indicate those cross-correlations with positive or negligible cross-correlation signal at $\tau > 10^{-4}$. Triangle annotations (△) indicate those cross-correlations with peaks on the timescale of the autocorrelation decay ($10^{-4} < \tau < 10^{-1}$)

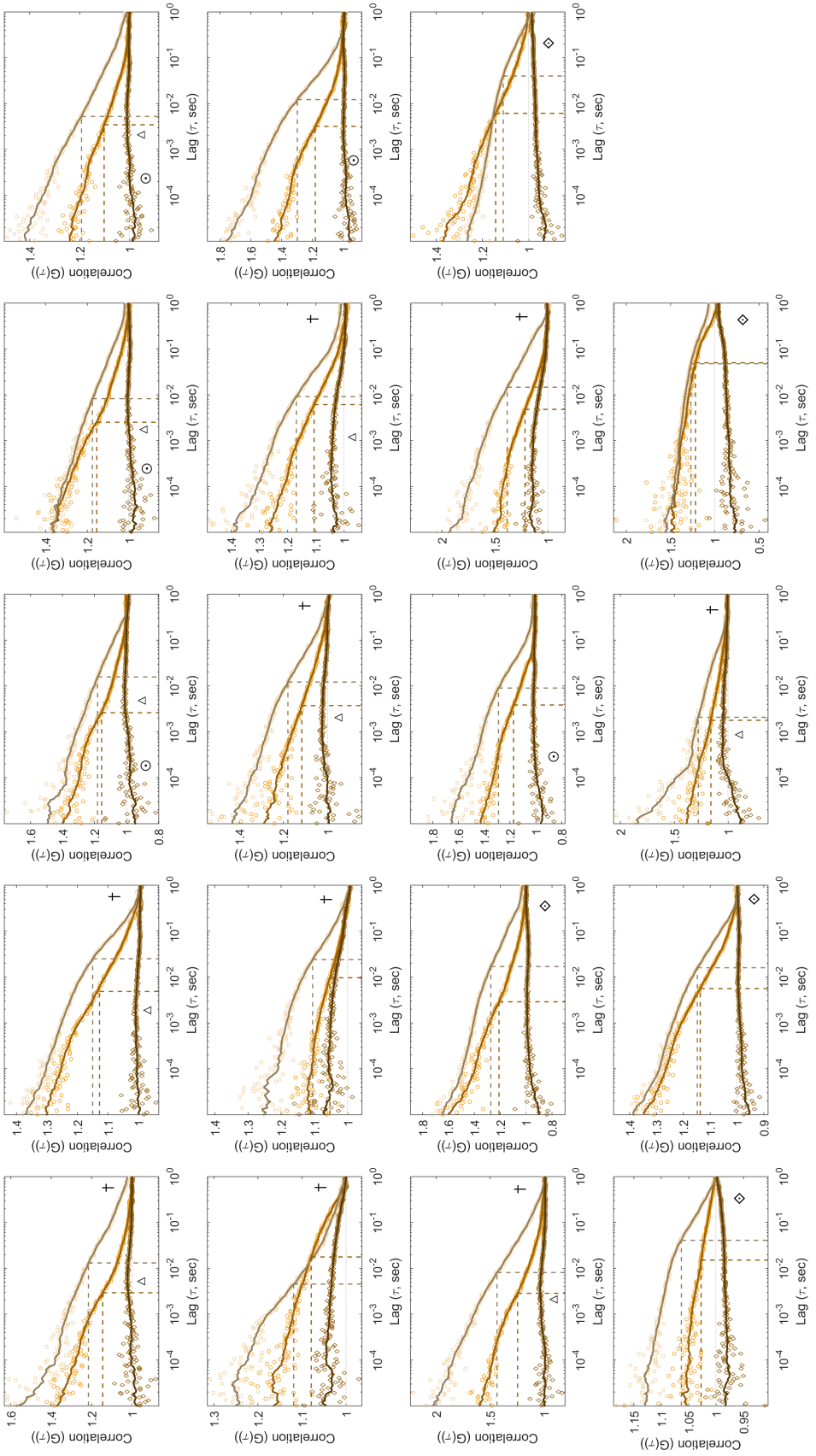

Figure S4: **Correlation results from LatB-treated cells stained with NR12S**. Dagger annotations (†) indicate those cross-correlations with positive or negligible cross-correlation signal at $\tau > 10^{-4}$. Triangle annotations (△) indicate those cross-correlations with peaks on the timescale of the autocorrelation decay ($10^{-4} < \tau < 10^{-1}$). Data sets showing anti-correlations becoming positive at or before the timescale of $\tau < 10^{-4}$ sec are indicated by circle dot annotations (⊙). Those data sets with anti-correlations across $10^{-5} < \tau < 10^{-0}$ timescales are indicated by diamond dot annotations (◈).

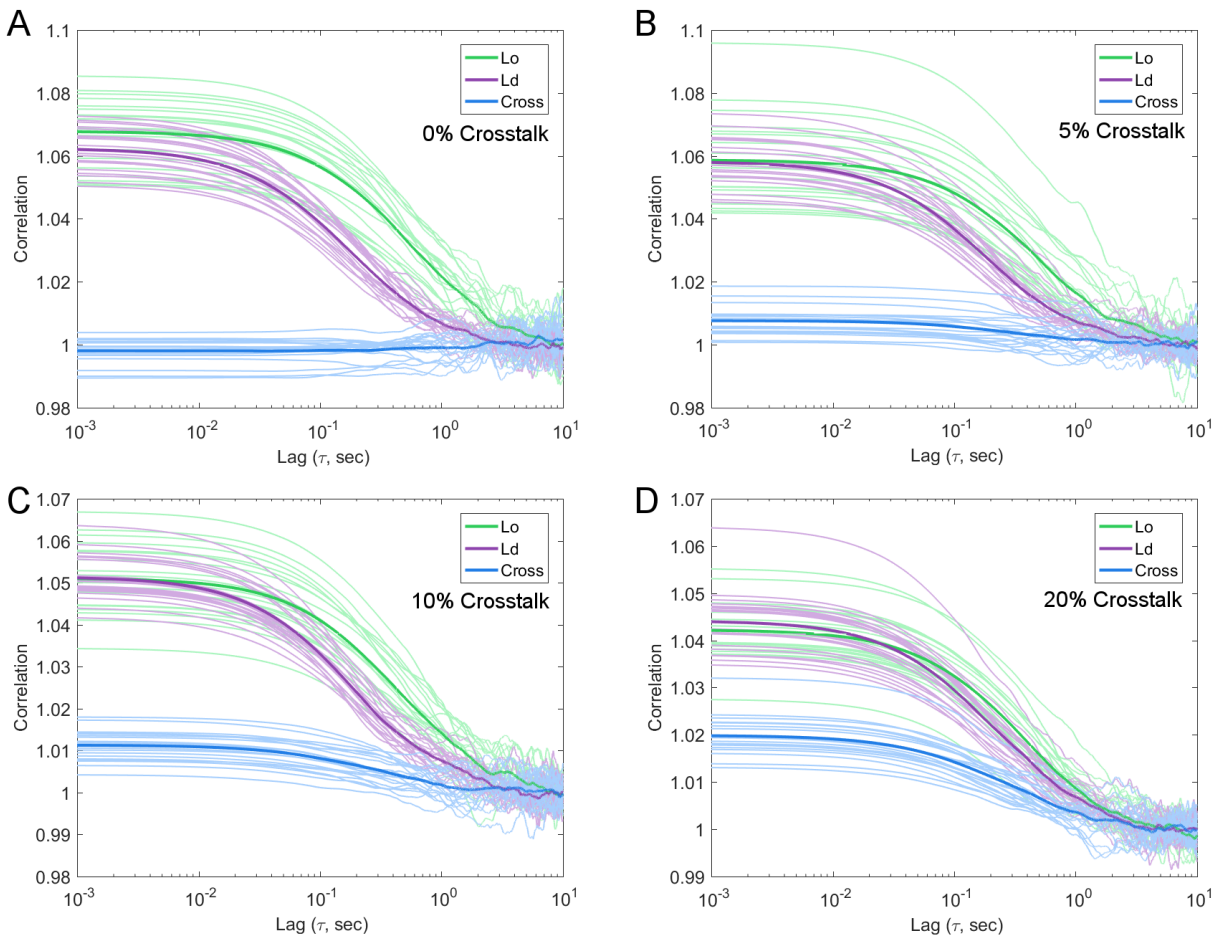

Figure S5: **Results of simulations with increasing amounts of crosstalk.** Simulations were run with probe identity assigned at the beginning of the experiment and retained through the entire run. This identity was assigned as 0 or 1, corresponding to fully L_o or L_d character in trial A. The subsequent trials assigned identity as 0.05 or 0.95 (B), 0.1 or 0.9 (C), or 0.2 or 0.8 (D). Propagating these assignments through to the intensity generation step of the simulation generated the 5%, 10%, or 20% crosstalk indicated. Panels A and D here appear as Figures 2A and 2B in the manuscript. Crosstalk reduces contrast between autocorrelation curves and gives a cross-correlation curve qualitatively similar to the autocorrelation curves.

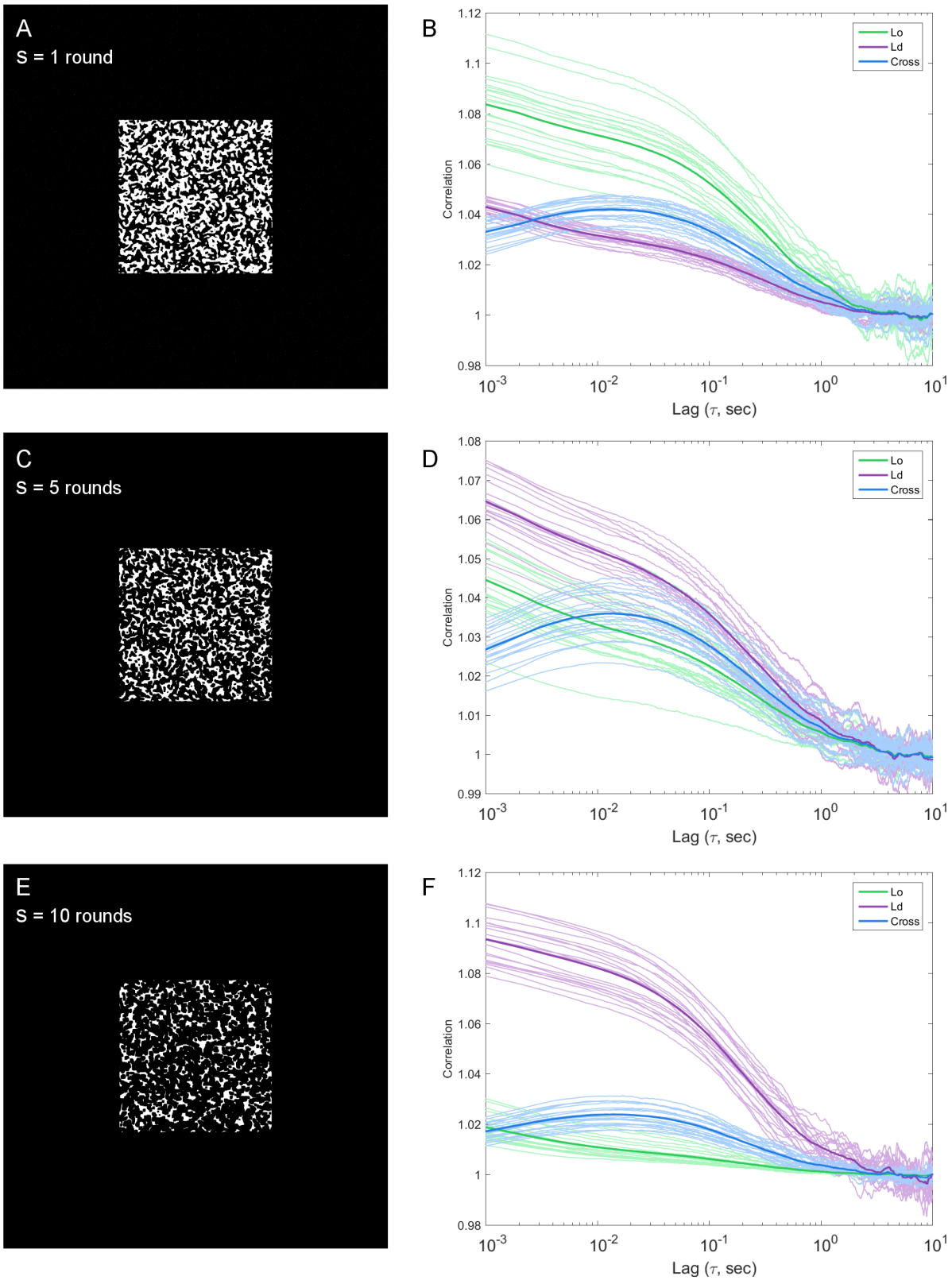

Figure S6: **Results of simulations with varying ratio of domain abundance.** A model membrane favoring one phase abundance over the other was generated by eroding a biphasic lattice of equal phase abundance (equivalent to those in manuscript Figures 2C, 3A, and 4 and SI Figure S7) and performing a morphological erosion operation. The erosion was performed with a square kernel of 3 x 3 pixels; the three conditions vary by how many rounds this erosion was performed. Example generated membranes appear at left with the corresponding correlation results from 20 rounds of probes diffusing in these environments at right. Varying domain abundance retains the qualitative features of the correlation curves though amplitudes of the L_o and L_d autocorrelation curves are altered. Note the amplitude of the cross-correlation curve remains between the two autocorrelation curves.

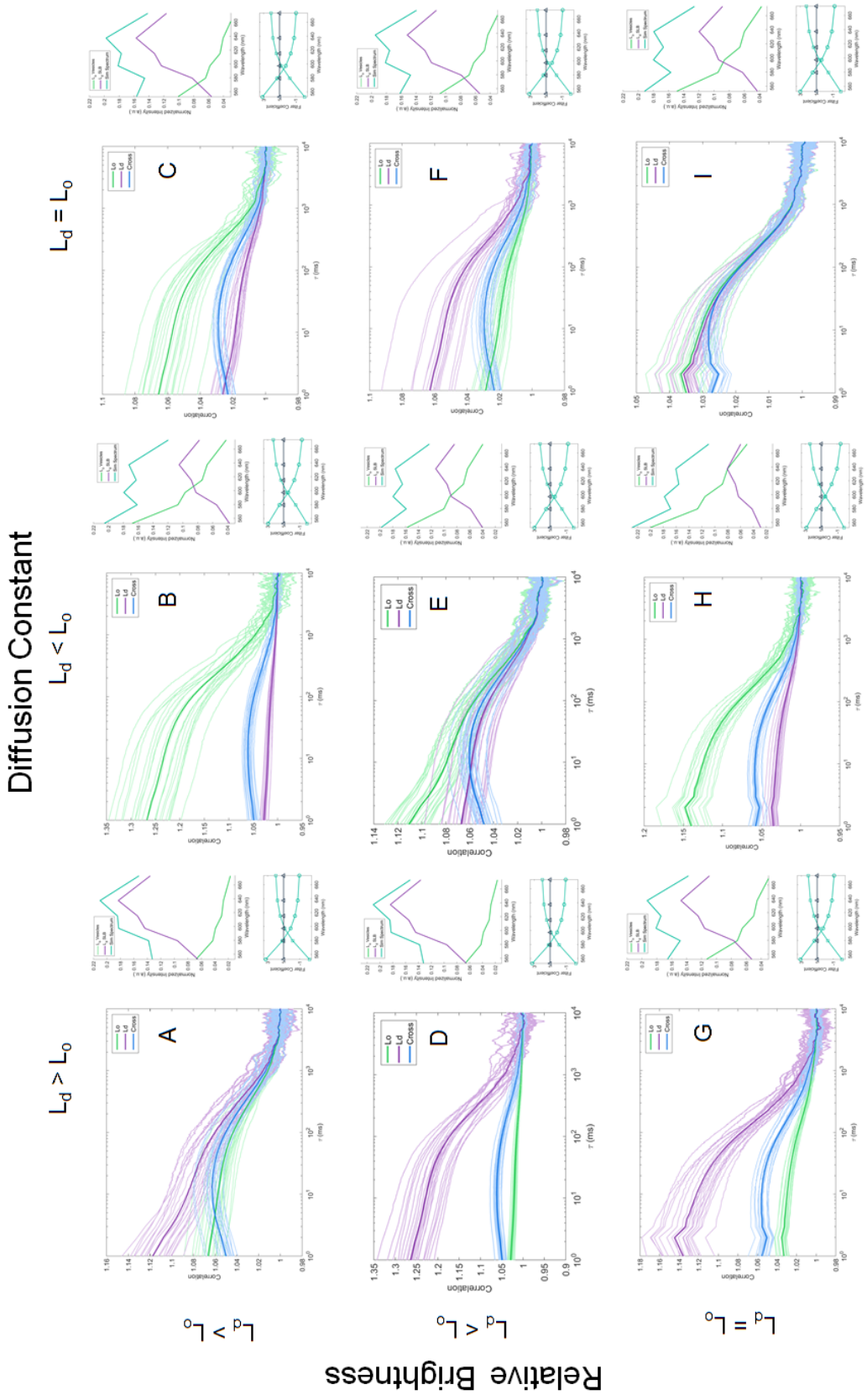

Figure S7: **Results of simulations comparing probe brightness and diffusion constant.** Simulations were run for probes diffusing within a static biphasic membrane lattice (equivalent to manuscript Figure 2 C and D conditions. Diffusion constant was either 0.1 or 0.3 $\mu m^2/sec$. Relative brightness per probe was set to either 1:1 (equivalent), 2:1, or 1:2 for probes in the L_d and L_o phase, respectively. Correlation curves, spectra, and filter coefficients for the 9 condition combinations are shown. The case shown in (G) most closely matches the autocorrelation amplitudes observed in experimental data.

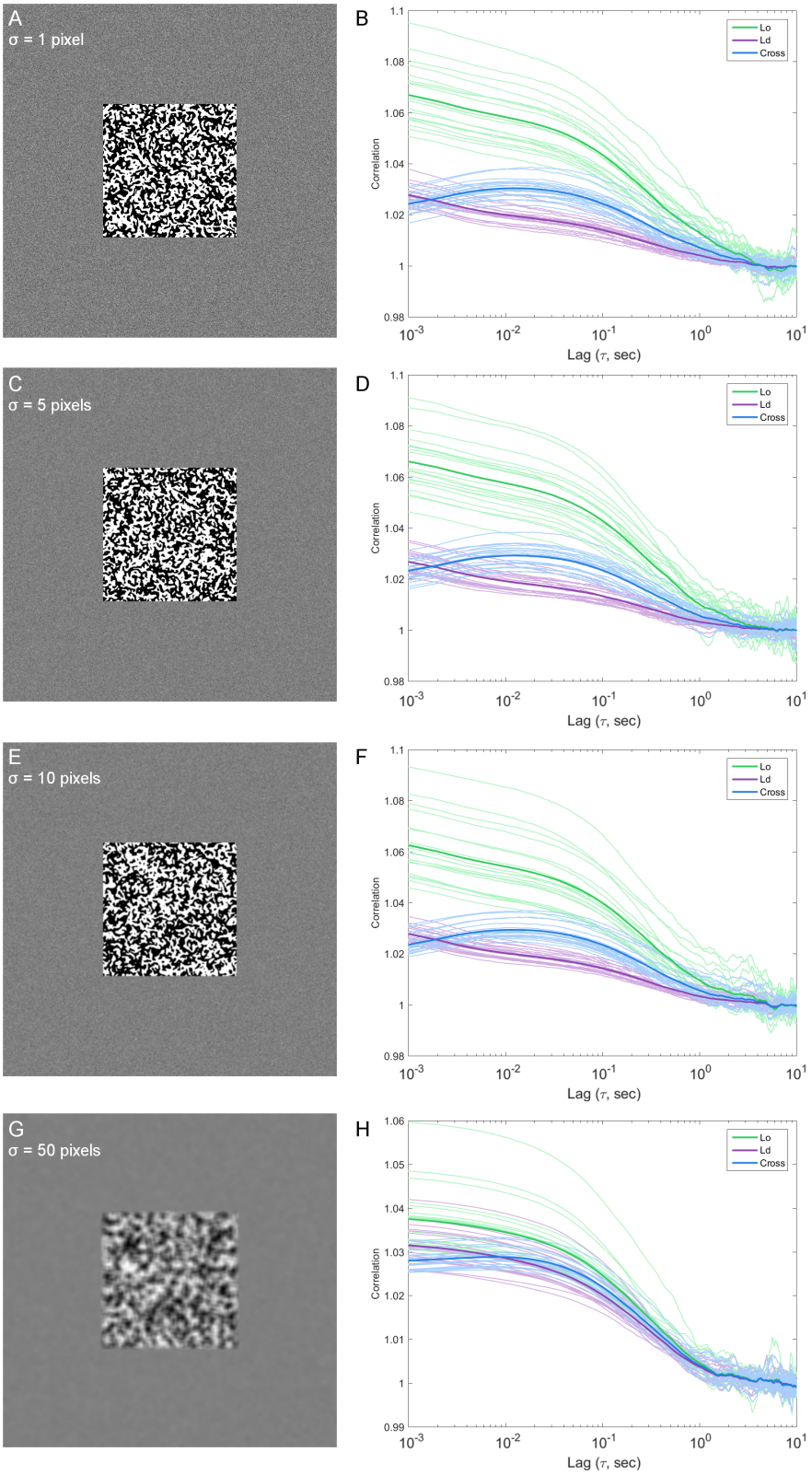

Figure S8: **Results of simulations with varying ratio of domain identity blurring.** A model membrane including gradients between full L_o and L_d character was used in place of a binary biphasic membrane environment; a binary environment appears in manuscript Figures 2C, 3A, and 4 and SI Figures S7 and S6. The gradient membrane was generated by modeling a binary lattice in identical manner to Figure 2C and blurring by a Gaussian kernel of width indicated by σ for each trial. Example modeled environments appear at left with the corresponding correlation results from 20 rounds of probes diffusing in these environments at right. The reduction in contrast between modeled L_o and L_d domains reduces contrast between the correlation curves but does not alter the qualitative features of these curves or their relative amplitudes.

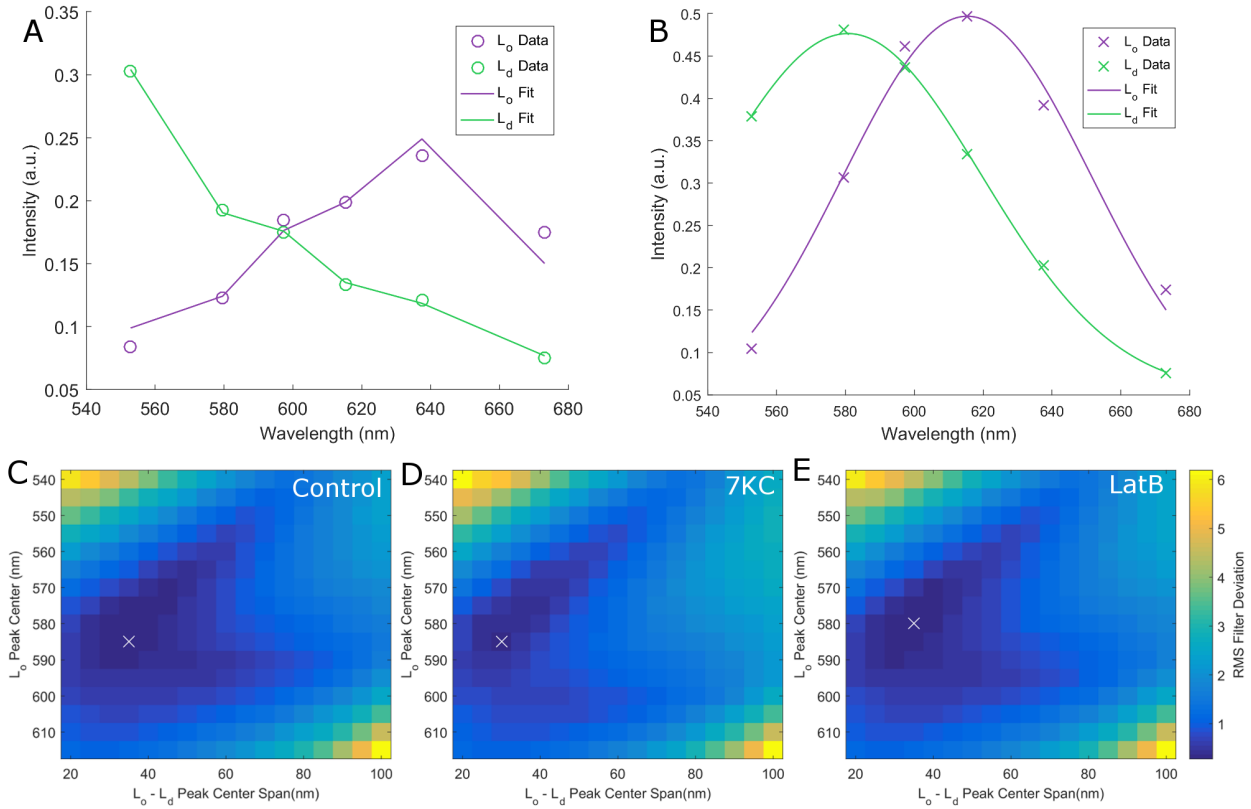

Figure S9: **Results of analysis to determine fitness of chosen basis spectra.** Spectra of NR12S in model membrane systems were fit to Gaussian curves. Panel A shows data as collected and presented in main manuscript; Panel B shows same data as in A but corrected for inhomogeneous spectral bin width of collected spectra. These fit curves were used to fit representative experimental spectra from live cells. Those trials yielding the lowest errors are indicated by white 'x' marks; these fall within 1 bin of the fits to the original experimental spectra.